Energy & Environmental Science

Understanding Cation Effects in Electrochemical CO_2 Reduction

Journal:	*Energy & Environmental Science*
Manuscript ID	EE-ART-04-2019-001341.R1
Article Type:	Paper
Date Submitted by the Author:	11-Jun-2019
Complete List of Authors:	Ringe, Stefan; Stanford University, Chemical Engineering Clark, Ezra; Technical University of Denmark, Joint Center for Artificial Photosynthesis Resasco, Joaquin; University of California Santa Barbara, Department of Chemical Engineering Walton, Amber; University of California, Chemical and Biomolecular Engineering Seger, Brian; Danish Technical University, Physics Bell, Alexis; University of California, Chemical and Biomolecular Engineering Chan, Karen; Technical University of Denmark, CatTheory Center, Department of Physics

Understanding Cation Effects in Electrochemical CO_2 Reduction

Stefan Ringe [b),],[1,2,a)] Ezra L. Clark,[3,4,b)] Joaquin Resasco,[5] Amber Walton,[3] Brian Seger,[4] Alexis T. Bell,[3] and Karen Chan[6,c)]

[1)] *SUNCAT Center for Interface Science and Catalysis, Department of Chemical Engineering, Stanford University, Stanford, California 94305, United States*

[2)] *SUNCAT Center for Interface Science and Catalysis, SLAC National Accelerator Laboratory, Menlo Park, California, 94025, United States*[b)]

[3)] *Joint Center for Artificial Photosynthesis, Lawrence Berkeley National Laboratory, Berkeley, CA 94720, United States*

[4)] *Surface Physics & Catalysis (SurfCat), Department of Physics Technical University of Denmark*

[5)] *Department of Chemical Engineering, University of California, Santa Barbara, Santa Barbara, California 93117, United States*

[6)] *CatTheory Center, Department of Physics, Technical University of Denmark, Kongens Lyngby 2800, Denmark*

(Dated: 11 June 2019)

Solid-liquid interface engineering has recently emerged as a promising technique to optimize the activity and product selectivity of the electrochemical reduction of CO_2 . In particular, the cation identity and the interfacial electric field have been shown to have a particularly significant impact on the activity of desired products. Using a combination of theoretical and experimental investigations, we show the cation size and its resultant impact on the interfacial electric field to be the critical factor behind the ion specificity of electrochemical CO_2 reduction. We present a multi-scale modeling approach that combines size-modified Poisson-Boltzmann theory with *ab initio* simulations of field effects on critical reaction intermediates. The model shows an unprecedented quantitative agreement with experimental trends in cation effects on CO production on Ag, C_2 production on Cu, CO vibrational signatures on Pt and Cu as well as Au(111) single crystal experimental double layer capacitances. The insights obtained represent quantitative evidence for the impact of cations on the interfacial electric field. Finally, we present design principles to increase the activity and selectivity of any field-sensitive electrochemical process based on the surface charging properties: the potential of zero charge, the ion size, and the double layer capacitance.

BROADER CONTEXT

The electrochemical reduction of CO_2 has the potential to reduce greenhouse gas emissions while producing valuable fuels and industrially relevant chemicals. A central challenge for commercialization is the need for increased activity and selectivity of catalysts towards desired products. In recent years, electrolyte optimization has emerged as a new strategy for electrocatalyst design. In particular, the cation identity has been shown to have a significant effect on CO_2 reduction (CO_2R) towards valuable products. In this joint experimental-theoretical work, we develop a multi-scale, continuum/ab initio modeling approach that shows the cation specificity to arise from differences in cation-cation repulsion and corresponding differences in the interfacial field. This model shows an unprecedented quantitative agreement with a wide range of experimental observations. The findings also show the hitherto neglected interfacial charging properties in determining the electrocatalytic activity for CO_2R and beyond and pave the way for electrolyte- and interface- engineering for general field-sensitive electrochemical processes.

[a)] Electronic mail: sringe@stanford.edu

[b)] Contributed equally to this work.

[c)] Electronic mail: kchan@fysik.dtu.dk

INTRODUCTION

Solid-liquid interface engineering has emerged in recent years as a promising technique to optimize the reactivity and selectivity of electrochemical reactions. In recent years, a number of engineering approaches have been explored, going beyond the design of catalyst's electronic structure towards a full optimization of the reaction environment.[1] For instance, researchers have investigated the effect of interfacial electric field,[2–6] pH[7–11] mass transport,[12–16] catalyst nano-structuring,[15,17–25] and the electrolyte composition, such as the solvent,[26–28] the buffer,[29–32] or the cations.[4,33–47] In particular, the identity of cations in the electrolyte has been shown to drastically affect the catalytic conversion rate in a number of critical electrochemical processes, such as the oxidation of water,[34,48] CO[35], formate[36], chloride,[37] hydrogen or alcohols[38,47], and in the reduction of oxygen[38,39,48] and CO_2[4,40–45]. The reduction of CO_2 (CO_2R) has been shown to be particularly sensitive to cation identity, with 1-3 orders of magnitude difference in activity between Li^+ and Cs^+ containing electrolytes. This effect has been demonstrated on Ag for the conversion to CO and on Cu towards the formation of hydrocarbons and alcohols containing multiple carbon atoms ("C_{2+}").[4,44]

The present joint theoretical-experimental study focusses on the mechanism behind cation specificity in the electrochemical reduction of CO_2R, as a case study for

general ion-specific electrochemical processes. The origin of cation effects on CO_2R has been contentious in recent literature. Hydrated cations were suggested to act as proton donors[49] and to modify the local electrode pH through shifts in local potential at the outer Helmholtz plane[41,44] or through acting as a buffer close to the electrode[45]. Cation-adsorbate interactions have been further suggested to occur via non-covalent chemical interactions.[38,39,48] It has also been suggested that alkali cation effects in CO_2R arise from chemisorbed ions.[50,51] However, we note that alkali ion adsorption including charge transfer is unlikely due to their very negative reduction potentials (≈-3 V vs. Standard Hydrogen Electrode (SHE)[52]).[33,37,38]

The plethora of hypotheses for cation effects in CO_2R effects highlights a pressing need for microscopic insight using computational simulations. Ions at the electrochemical interface are particularly challenging to treat from an *ab initio* perspective, as their slow motion compared to water and large solvation shells introduce many degrees of freedom and associated sampling challenges. On the other hand, continuum models of the electric double layer have a long history[53–55], and have yet to be exploited in recent theoretical investigations of ion effects.

Recent studies from our groups demonstrated that cations affect the CO_2R activity through their electrostatic interactions with the electric dipole of specific adsorbates[3,4]. Here, we build upon these studies, taking a mean-field electrostatic approach and modeling the electrolyte distribution with a modified Poisson-Boltzmann model.[56] We find that the surface charge density and electric field is reduced by ion-size dependent hydrated cation repulsions at the outer Helmholtz plane. We perform surface charge-dependent Density Functional Theory calculations of reaction intermediates in order to relate the ion-specific surface charge differences to differences in electrocatalytic activity. The resulting multiscale approach is evaluated with a wide range of ion-specific experimental data: CO production on various epitaxial surface facets of Ag, C_2 formation on epitaxial Cu, the vibrational stretching mode of *CO on polycrystalline Pt and Cu as well as impedance data on single crystal Au(111) electrodes. Using a single set of experimentally motivated cation size parameters, we obtain unprecedented *quantitative* agreement with all experiments, which suggests the validity of the simple picture presented. Finally, we present cation and system design principles based on the optimization of the surface charge density and electric field, which we envision to have general applicability to electrocatalytic processes beyond CO_2R.

MODEL FORMULATION

Modeling Cation Effects – the ai1c approach

Figure 1 outlines our combined *ab initio*/continuum approach to modeling ion specific electrocatalytic activity. This approach is motivated by the previously noted strong double layer electric field-dependence of critical reaction intermediates in CO_2R.[3–5,57] As illustrated in the right panel of Figure 1, we determine the surface-charge density dependence of the energetics of critical reaction intermediates via charged implicit solvent corrected DFT calculations using a planar countercharge[58]. These energies are then related to reaction rates through a simple rate-limiting step approximation. As later described in more detail, we then find $\Delta\mu(\sigma)$ to be largely independent of the counter charge distribution. This important observation suggests that cations affect catalytic activity by a change of the surface charge density at a fixed electrode potential.

In order to describe the variation of surface charge density σ as a function of cation type and applied electrode potential, we apply a continuum electrolyte model, the size-modified Poisson-Boltzmann (MPB) approach (cf. left panel in Figure 1)[56]. As illustrated in Figure 2, the model predicts that cations with a smaller hydration shell like Cs^+ are more concentrated at the electrode compared to larger cations like Li^+. This difference in concentration increases the surface charge density and the field at a given potential relative to the potential of zero charge (PZC) $\phi^{\mathrm{M}} - \phi^{\mathrm{M,PZC}}$. The continuum model provides us with the dependence of the surface charge density on potential and ion size a, $\sigma(\phi^M - \phi^{\mathrm{M,PZC}}, a)$. Coupling the $\Delta\mu(\sigma)$ determined through DFT with $\sigma(\phi^M - \phi^{\mathrm{M,PZC}}, a)$ we obtain the dependence of catalytic activity on ion size.

The present model differs from previous work in several significant ways. The primary hypothesis here is that cation effects in CO_2R are mean-field in nature, in contrast to previous studies that consider cation effects to arise from explicit interactions of cations with key reaction intermediates.[3,4,46,51] . Furthermore, we model the impact of ion size on the double layer structure independently from the *ab initio* simulations of the reaction energetics.

There are several advantages to this modelling approach. Since the reaction energetics are determined independently of the double layer model, a given $\Delta\mu(\sigma)$ from a single *ab initio* simulation can be coupled with a variety of detailed continuum double layer models, and even with experimental capacitance data. This flexibility is not possible with constant potential grand canonical DFT simulations which include complex electrolyte descriptions directly in the DFT setup[6,59–69] making it difficult to derive the correct functional forms or parameters.[65,70] Furthermore, constant potential grand canonical DFT simulations require a reference to relate the simulated work function to potential. Typically the reference that is applied is the work function of the stan-

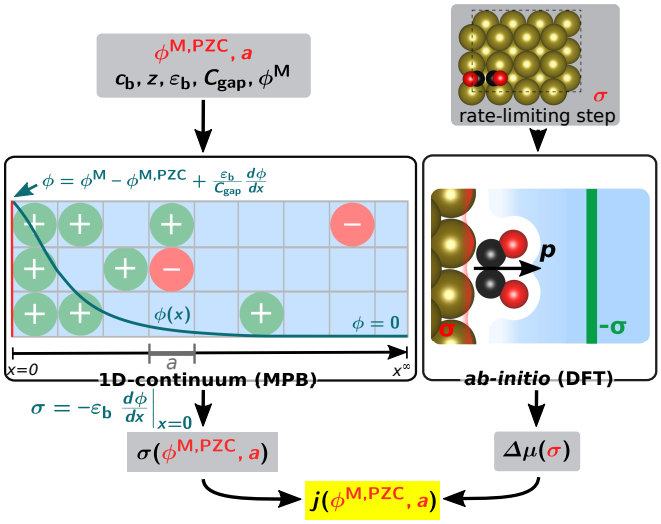

FIG. 1: Schematic illustration of our multi-scale modeling approach to model cation effects on field-driven electrocatalysis. The process of surface charge generation as a function of potential (left panel) is simulated by a 1D-continuum electrostatic description of the electrolyte. The ion-size modified Poisson-Boltzmann approach (MPB) enables us to model the effect of ion size on the generated surface charge at a fixed potential. Surface charge density dependent reaction energetics are obtained from charge-dependent DFT calculations of the rate-limiting species (right panel). Combining the results via interpolation, we obtain the catalytic activity or current density as a function of cation size and potential of zero charge at fixed applied potential.

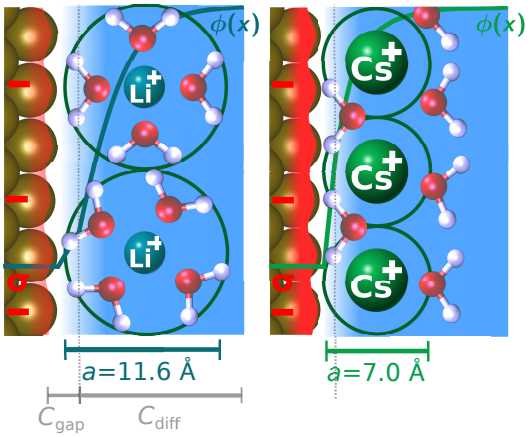

FIG. 2: Illustration of the origin of cation effects in field-driven electrocatalysis as suggested by this work. Repulsive interactions between hydrated cations at the outer Helmholtz plane reduce the local concentration of cations, the surface charge density σ (depicted by the red-colored region) and the electric double layer field. The diffuse layer that is explicitly modeled by the MPB model is depicted as well as the Helmholtz gap capacitance region and the interfacial ion diameter determined in this work.

dard hydrogen electrode, which has been reported to have a range from 4.3 to 5.3 eV.[71–76] Here our approach allows us to use the PZC of a given metal|solution interface as a reference, which can have a higher accuracy than the SHE reference in well-characterized metals.

In what follows, we lay out the details of the model.

Continuum Surface Charging Model

The electrostatic potential ϕ in a solution is described by the one-dimensional Poisson equation

$$\varepsilon_b \frac{d^2\phi}{dx^2} = -\sum_i z_i c_i[\phi] \quad , \tag{1}$$

where ε_b is the bulk dielectric permittivity (in units of the vacuum permittivity) and z_i and c_i refer to electrolyte species changes and concentrations. We apply finite ion-size modified version of the Poisson-Boltzman model, which for a z:z electrolyte is[56]:

$$c_\pm[\phi] = c_b \frac{e^{\mp \frac{z_i F \phi}{RT}}}{1 - \chi_0 + \chi_0 \cdot \cosh\left(\frac{z_i F \phi}{RT}\right)} \quad , \tag{2}$$

with the Faraday and ideal gas constants F and R, the temperature T, the ionic charges z_i, the ionic bulk concentration c_b and the ion-occupied volume fraction $\chi_0 = 2c_b a^3 N_A$, with the Avogadro constant N_A and the lattice cell length a. This expression arises from a statistical lattice model in which each anion and cation is only allowed to occupy a single cell (cf. Figure 1). This restriction effectively leads to a maximum possible ion concentration determined by χ_0. a denotes a lattice cell length in the statistical model is equivalent to an effective ion diameter if ions are considered as hard particles. In this picture, the distance of the cation from the electrode will directly correspond to $a/2$ (cf. Figure 2) which has been determined experimentally by x-ray scattering and diffraction methods[39,77–81]

Interestingly, a comparison of experimentally tabulated electrode-cation distances suggests these to be only slightly dependent on the applied potential and metal electrode. In the case of Cs^+, a distance of around 3.5 Å has been determined at both the Au(111)[81] and Pt(111)[79] electrodes. K^+, which is a harder cation with a larger hydration shell in the bulk electrolyte,[82] was found to at larger distances of 4.1 Å to the Ag(111) electrode.[77] These results suggest that ion sizes are relatively invariant on different metal surfaces. In the following, we use these two experimentally determined values while values for other cations are inter- and extrapolated from experimental measurements.

The MPB equation is solved with the following boundary conditions (cf. also Figure 1). At the bulk electrolyte boundary ($x = x^\infty$, multiple μm), we apply the Dirichlet

boundary condition $\phi = 0$. At the electrode side $x = 0$, we apply the Robin boundary condition:[83,84]

$$\sigma = -\varepsilon_{\mathrm{b}} \cdot \frac{d\phi}{dx}(x=0) = C_{\mathrm{gap}} \left[\phi^{\mathrm{M}} - \phi^{\mathrm{M,PZC}} - \phi(x=0)\right] \quad , \tag{3}$$

where ϕ^{M} is the metal electrode potential relative to the bulk electrolyte and C_{gap} is an interfacial Helmholtz-like capacitance which acts in series with the diffuse layer capacitance. This mixed boundary condition allows us to correctly describe surface charging at potentials far from the PZC, where the gap capacitance C_{gap} dominates the surface charging response. Physically, C_{gap} arises mostly from Pauli repulsion of the electrons, which creates a vacuum-like gap between solid and liquid (cf. Figure 2).[85–87] This boundary condition also has the practical advantage of offering a direct link between surface charge density and electrode potential, which is determined by the macroscopic properties of the electrode as the PZC and the Helmholtz gap capacitance (cf. Figure 1). We note that $x = 0$ corresponds here precisely to the outer part of the Helmholtz gap, as illustrated in Figure 2.

Experimentally, the value of the double layer capacitance C_{dl} at negative potentials far from the PZC has been found to be approximately facet-independent on Ag,[88] and is very often independent of metal identity.[89,90] C_{dl} was measured to be around 20-25 μF/cm^2 for Ag surfaces ,[88,91–93] Cu(111)[94] and Pt(111)[95]. At potentials far from the PZC, the gap capacitance dominates, which is why we apply a value of $C_{\mathrm{gap}} = 25\,\mu$F/cm^2 throughout the paper. Finally, experimental PZC's have been used to parametrize Eq. 3 as listed in Table I with the exception of the pc-Ag surface, where we used a theoretical estimate due to the diversity of the experimental data (cf. Supplementary Materials). Solving the MPB equation then gives the relation $\sigma(\phi^{\mathrm{M,PZC}}, a)$, which is shown in Figure S1 of the Supplementary Materials.

Ab initio derived field dependent electrocatalysis

As mentioned before, dipolar and polarizable intermediates, such as *CO_2 or *OCCO, interact significantly with electric double layer fields.[3,4] The dependence can be derived from surface charge-dependent DFT calculations. The electrolyte counter charge can be represented by either explicit cations[3,96,97] or a continuum representation as implemented into various DFT program packages.[61–64,67–69] We here applied a mean-field formulation using both a planar counter charge (PCC) as well as a linearized PB (LPB) representation. Figures S2 and S3 of the Supplementary Materials show the dependence of the free energy change $\Delta\mu$ for CO_2 adsorption on Ag on σ. $\Delta\mu$ is dependent on neither the electrolyte model (i.e. LPB or PCC) nor the location of the counter-charge in the PCC model (cf. Figure S3). This observation is critical since it shows that, at least in a mean-field approximation, cation affect reaction kinetics via a change of the surface charge density.

The $\Delta\mu(\sigma)$ function obtained from DFT is nearly parabolic, which in the case of a field-dependent expression arises from both the first order dipole interaction and the 2nd order polarizability.[4,98] Therefore we can obtain an analytic expression by interpolation the surface charge density dependent formation energies with the parabolic function:

$$\Delta\mu(\sigma) = \Delta\mu(\sigma=0) + a_\sigma\sigma + b_\sigma\sigma^2 \quad . \tag{4}$$

The accuracy of this approach is demonstrated in Figures S2–S9 in the Supplementary Materials, where the parabolic function nearly perfectly fits the calculated DFT data points as a function of surface charge density.

In this work, we investigate cation effects on CO_2R at Ag and Cu as well as CO adsorption on Pt. For each of these cases, the current density is expressed in our model as determined by the formation energy of the rate-limiting species. For CO_2 at Ag, recent literature suggested CO_2 adsorption with concomitant electron transfer to limit the CO production rate.[57,99–102] Spectroscopic studies on Ag[103] and Cu[104] have also identified carboxylate intermediates. As shown in Figure S2, *CO_2 is strongly stabilized by electric double layer fields. This is also clear from the field-corrected free energy diagram given in Figure S10 that also suggests that CO_2 adsorption limits the CO production rate in accordance with the literature. Furthermore, recent theoretical results have shown that the transition state of the CO_2 adsorption process is close to the final state.[105] The CO partial current density j_{CO} can thus be expressed as a function of the *CO_2 adsorption energy at standard conditions $\Delta\mu_{*\mathrm{CO_2}}$:

$$j_{\mathrm{CO}} \propto \exp\left(-\frac{\Delta\mu_{*\mathrm{CO_2}}(\sigma)}{RT}\right) \quad . \tag{5}$$

In the following, we will consider the partial current density normalized to a particular cation which represents the cation effect on the turn over frequency removing the need to specify an active site density. In the case of CO_2 reduction on Cu, the most significant cation effects were observed for C_2 product formation. From previous studies, the CO-CO coupling step has been discussed to limit the corresponding production rate.[3,7,30,106–108] Similar to CO_2 adsorption, CO-CO coupling is a chemical step which is driven by interfacial field stabilization of the dipolar adsorbate (*OCCO).[3] This dipole-field interaction results in a large surface charge dependence as shown in Figure S7. We assume a similar dipole for the coupling transition state as in the final *OCCO state, resulting in the C_2 production rate expression as a function of the *OCCO energy relative to the bare surface, $\Delta\mu_{*\mathrm{OCCO}}$:

$$j_{\mathrm{C_2}} \propto \exp\left(-\frac{\Delta\mu_{*\mathrm{OCCO}}(\sigma)}{RT}\right) \quad . \tag{6}$$

Ag(111)	Ag(110)	pc-Ag	Cu(111)	Cu(100)	CO@Pt(111)	pc-Au
-0.45	-0.734	-0.584	-0.2	-0.54	1.1	0.16

TABLE I: Experimental Potential of zero charges (PZC) vs. SHE for the different surfaces that were used in this work.[109,110] Only the pc-Ag value was estimated from theoretical considerations (cf. Supplementary Materials).

Cs	Rb	K	Na	Li	TMA	TEA	TPA	TBA
3.5	3.9	4.1	5.2	5.8	7.8	8.0	8.1	8.4

TABLE II: Obtained effective interfacial cation radii ($a/2$ in Å) from experiment[77,79,81] (K^+ and Cs^+) and inter-/extrapolation to fit the experimental data of CO_2R to CO at Ag surfaces and CO electrochemical Stark shift at Pt.

RESULTS & DISCUSSION

Cation effects on CO_2R

In what follows, we evaluate the model against the experimentally observed ion-specificity of CO_2R on two surfaces, Ag and Cu. Figure 3 shows the theoretical (lines) and experimental (dots) shifts in activity towards CO at -1 V vs. RHE for Ag(111), Ag(110), and pc-Ag, where the first two surfaces are epitaxial thin films .[4,5]. The activity data is normalized to that of Li^+ (cf. Figure S19 in the Supplementary Materials for full polarization curves).

As seen from the comparison, the model gives essentially quantitative agreement with experiment. Cations such as Cs^+ have the smallest hydrated cation radius and therefore show the smallest repulsion close to the electrode. The resulting higher concentrations of cations lead to a larger surface charge density and stronger interfacial electric field, which drives the adsorption of CO_2, as illustrated in Figure 2 and 1.

The validity of our mean field approach is further supported by the correct prediction of the facet dependence of cation effects. Recent work has suggested that carefully grown epitaxial thin films exhibit a small number of step defects[5,103], which predominate in the activity of both Ag and Au electrodes.[5,111] Since the dipole moments of the adsorbates involved are essentially facet independent (cf. Figures S2 and S7 in the Supplementary Materials), the actual binding energies of the adsorbates do not come into play in determining the relative activities amongst the cations. Instead, it is the charging properties (PZC and capacitance) that determine ion specificity. As shown above, although step defects could exhibit specific charging properties,[2] activity trends still follow the charging properties of the dominating surface facet. The stronger cation effects at the Ag(111) facet can be rationalized by its more positive PZC and consequently its higher surface charge density and sensitivity to a change of cations (cf. also Figure S1 in the Supplementary Materials).

The observed cation dependence of the CO production rate indicates the efficiency of cation modulation for process optimization. In contrast, the small dipole of adsorbed *H atoms has been found before to result in a negligible electric field dependence[5]. The relative independence of the hydrogen evolution rate (cf. Figure S4 in the Supplementary Materials) suggests that the dipole of the corresponding transition state is also significantly

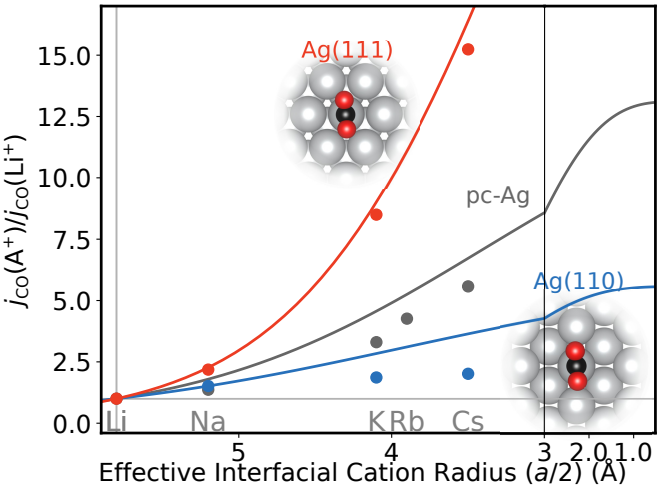

FIG. 3: CO partial current density at Ag(110), Ag(111) and poly-crystalline Ag at -1 V vs. RHE for different cations normalized to the CO current density in the Li^+ case. Filled circles represent the experimental data points, solid lines the theoretical prediction. The Ag(110) data is plotted relative to the Na^+ cation due to possible impurities in the Li^+ measurement (cf. Supplementary Materials).

smaller. Resasco *et al.* have further shown that the formate production rate behaves similarly among exchange of cations as CO,[4] suggesting CO_2 adsorption to also be the limiting step for that process as well.

We now turn to the effect of cations on the activity on Cu epitaxial thin films which has been studied by Resasco *et al.*[4] . Similar to Ag, no cation effects were observed for hydrogen evolution reaction, which we again attributed to the small dipole and polarizability of adsorbed H atoms. By contrast, strong cation effects on C_2 formation were observed, which can be attributed to the large dipole of the critical *OCCO intermediate. Figure 4 shows a comparison of the theoretical and experimental relative activities, and again a surprisingly good agreement of the theoretical prediction with the experimental results is obtained, with slight deviations for Cs^+. Dynamic interactions with *OCCO may give an additional stabilization of *OCCO as seen from explicit DFT calculations,[46] leading to the direct impact of cations on formation energies, which has not been considered here. The stronger cation effects on the Cu(111) surface can be again rationalized by the more positive PZC compared to the Cu(100) facet. We stress that these results were ob-

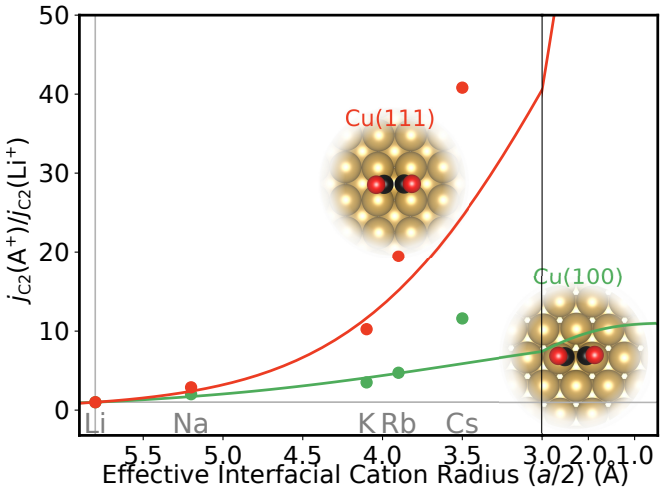

FIG. 4: Partial current density of C_2 products (ethanol and ethylene) at Cu(111) and Cu(100) at -1 V vs. RHE for different cations normalized to the C_2 current density in the Li^+ case. Filled circles represent the experimental data points, solid lines the theoretical prediction.

tained using exactly the same ion sizes as in the other two cases.

Cation effects on electrochemical CO Stark shift

Next, we considered CO adsorption on Pt surfaces, a system that has been well studied for electrochemistry.[35,87,110,112–120] Among the plethora of experimental insights that has been reported over years, it was found that the CO stretching vibration varies significantly with an applied field under ultra-high vacuum conditions.[115] This change in the CO vibration frequency with electric field has been understood as a result of the Stark effect, i.e. the interaction of applied electric fields with the CO vibrational mode.[115] Under electrochemical conditions, the interfacial field is controlled by the metal potential ϕ^{M}. The Stark tuning rate here, though, may be complicated by two factors: CO may bind to different sites at different potentials, and also at high coverages depolarization may occur.

The frequency shift with electrode potential can be expressed as a product of surface charge dependence of the frequency and surface charging contribution:

$$\frac{d\tilde{\nu}}{d(\phi^{\mathrm{M}}-\phi^{\mathrm{M,PZC}})} = \frac{\partial\tilde{\nu}}{\partial\sigma}\frac{d\sigma}{d(\phi^{\mathrm{M}}-\phi^{\mathrm{M,PZC}})} = \frac{\partial\tilde{\nu}}{\partial\sigma}C_{\mathrm{dl}} \quad . \tag{7}$$

We found the first part – which denotes the Stark tuning rate expressed as a function of σ – to be roughly constant with σ as depicted in Figure 5 a). More importantly, the figure also shows that $\frac{\partial\tilde{\nu}}{\partial\sigma}$ is nearly the same for CO at bridge and top sites at a fixed *CO coverage making it a function of the coverage alone (cf. Figure S15 in the Supplementary Materials). Experimental analysis of the *CO coverage has been performed in the past[110,112] suggesting it to adopt a fixed, saturated value of around 65% at negative potentials below -1 V vs. SHE.[110] Considering these results, the experimentally measured change of the CO stretching frequency reflects the pure Stark tuning rate without the effects of site-redistribution or coverage-dependent depolarization, in agreement with previous studies.[112,118]

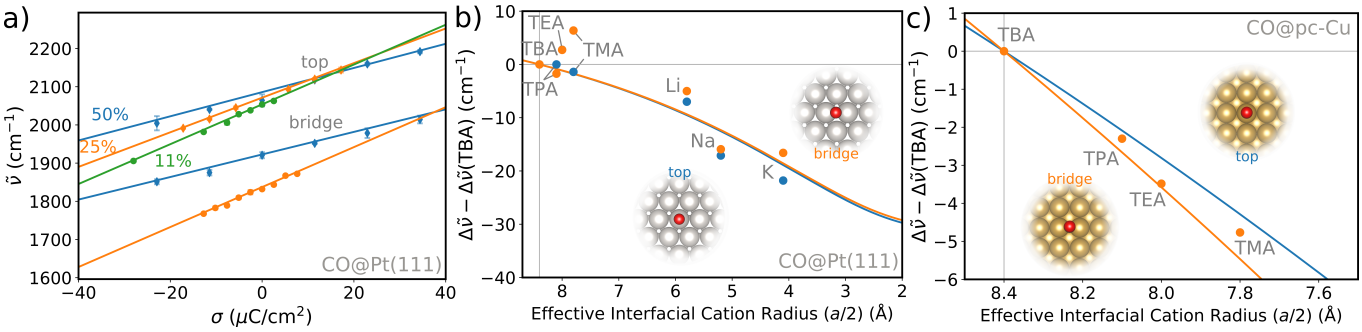

FIG. 5: a) *CO stretching vibrational mode shift on polycrystalline Pt as a function of surface charge density leading to the experimentally observed electrochemical Stark effect. The upper three lines refer to adsorption on top, the lower ones to adsorption on bridge sites. Different symbols and colors distinguish different CO coverages. b) Cation effect on the *CO stretching frequency. Filled circles represent absorbance maxima from the ATR-SEIRAS spectra of ref.[121] at -1.1 V vs. SHE, solid lines depict the theoretical prediction using the ai1c approach. c) *CO stretching vibrational mode shift on polycrystalline Cu as a function of surface charge density. Filled circles represent the ATR-SEIRAS data of ref.[118] at -1.39 V vs. SHE, solid lines depict the theoretical prediction using the ai1c approach (using Cu(100) model surface).

Figure 5 b) shows the measured effect of cations on the *CO stretching frequency on Pt at -1.1 V vs. SHE (dots)[121] and the theoretical curve (lines) from the ai1c model. In order to simulate the trends with our model, we took the same ion radii as before for the alkali cations and additionally obtained the radii of TBA and TPA from a fit of our model to the experimental data in Figure 5. In the case of TEA and TMA, a direct fit would give ion sizes that are not following the expected size ordering of the organic cations (TMA ¡ TEA ¡ TPA ¡ TBA). A possible explanation for this could be inaccuracies in the experimental determination of the stretching frequency. In order to correct for this, we obtained the TEA and TMA sizes from correlating all cation sizes with experimental radii (cf. Figure 7), as discussed below. Using this strategy, we generally found good agreement with the experimental trends.

A similar experimental ATR-SEIRAS study has also considered the cation effect on the CO stretching vibration on a polycrystalline Cu electrode.[118] Assuming a coverage of around 50%, which has been found by *ab inito* based micro-kinetic modeling[7], we applied the same strategy as for Pt. Figure 5 c) shows again excellent agreement with the experimentally observed cation effect. The consistency between experimental and theoretical Stark shifts further supports the generality of our model and the developed understanding of cation effects.

Cation effects on surface charging

So far, we discussed that cation repulsion leads to a decrease of the surface charge density and corresponding double layer electric field. Figure 6 a) shows that for a Au(111) surface that this effect leads to the double layer capacitance decreasing with cation size at potentials away from the PZC (0.56 V vs. SHE[122]). We performed impedance spectroscopy on Au(111) single crystal electrodes using 0.05 M $KClO_4$ and $NaClO_4$ solutions to confirm this behavior. Independent of the circuit used for fitting, we found the double layer capacitance to decrease from Na^+ to K^+ as depicted in Figure 6 b) (cf. also Figures S12 and S13 in the Supplementary Materials). Indeed, the capacitance increase has been also observed in Monte Carlo simulations of the electric double layer[123] as well as impedance studies on single crystal electrodes[124] and supercapacitors.[125]

Finally, we note that previous studies suggested that cations also affect the PZC as well as capacitance close to the PZC.[124] In our data, we noticed a frequency dispersion close to the PZC, making a direct interpretation difficult. We also note that under the commonly applied highly negative potentials for CO_2R, the Helmholtz capacitance variation with ion size likely dominates the overall surface charge variation (cf. Figure 6 b). Finally, recent studies have found that cation effects do not depend on the cation concentration[120] which can be seen as further evidence that the diffuse layer region does not significantly contribute to the observed effects.

IMPLICATIONS FOR ELECTROCHEMICAL SYSTEM DESIGN

The sensitivity of CO_2R to the interfacial field suggests that the electrolyte and the charging properties of the interface can be used as design parameters towards electrocatalyst optimization. In order to estimate the limits of a cation screening approach, we plotted in Figure 7 the effective interfacial cation radii as a function of the experimentally measured ionic crystal radii.[82]. We find two separate nearly perfect correlations, one for the organic cations and one for the hydrated ones. The size of the solvated organic cations at the interface generally increases with their crystal ion radius.[112] Inorganic

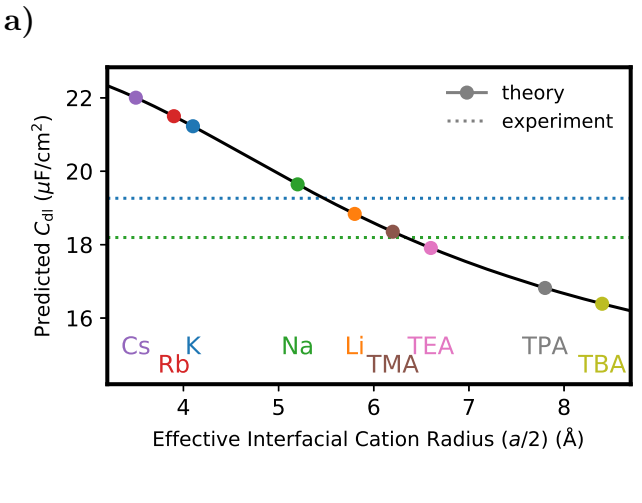

FIG. 6: Double layer capacitance at the Au(111) single-crystal electrode using a 0.05 M $KHCO_3$ or $NaHCO_3$ electrolyte. a) Potential-dependence of the double layer capacitance obtained from fitting a RC circuit to the impedance data. Filled circles denote the data points, the solid gray line the difference in surface charge density between both experiments under the assumption of the same PZC of 0.97 V vs. RHE.[122]. b) Solid black line: MPB model predicted double layer capacitance as a function of effective interfacial cation radius at 0 V vs. RHE. Values at the here determined interfacial radii are depicted by filled circles, the measured double layer capacitance for K^+ and Na^+ by the dashed lines.

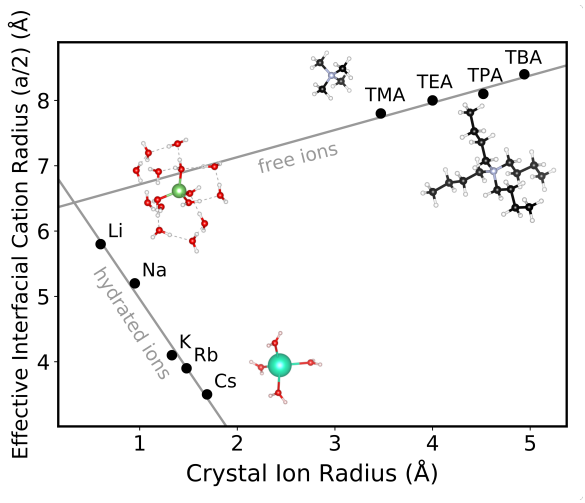

FIG. 7: Correlation of the effective interfacial cation radius obtained in this study with the crystal radius from Ref.[82]. The analytic expressions $-2.2 \cdot x + 7.6$ and $0.42 \cdot x + 6.3$ have been found to fit the cation correlation for hydrated and hydration-free cations, respectively.

cations, on the other hand, have relatively rigid solvation shells which scale inversely with the crystal radius, leading to a negative slope. In Figure S17 of the Supplementary Materials, we have simulated model predictions of the relative CO production rate resulting from both single-valent and multivalent hydrated inorganic ions using the obtained correlation. The net impact of multivalent ions arise from two competing effects; their larger charge would increase the interfacial field, while their larger sizes tend to decrease the field. We found several cations to exhibit up to two orders of magnitude higher activity than Cs. Ion-correlation effects[126] or chemical ion-adsorbate interactions could, however, lead to deviations of the estimations using our simplified model. One experimental study does suggest that lanthanides could exhibit a high CO production activiy.[127] This study also suggested a possible correlation of activity with the surface charge density, which our theory confirms. From an experimental perspective, multi-valent cations such as lanthanides or actinides would be interesting candidates, since their low standard reduction potential prevents them from adsorption under reducing CO_2R conditions, and they are furthermore soluble enough to provide sufficient ionic conductivity.

A second way to increase the conversion rate of electric field driven reactions is through modification of surface charging properties as the PZC or the gap capacitance. Experimental studies on CO adsorption on Pt for example have shown that adsorption of CO leads to a PZC increase from 0.23 to 1.1 V vs. SHE.[110] By performing DFT-based PZC calculations using implicit solvation, we found a similar increase but only for bridge bound *CO, while top site bound *CO was less sensitive (cf. Supplementary Materials Figure S11). The sensitivity of the PZC to surface adsorbate coverage was also shown for other systems[128] suggesting the possible use of co-adsorbates during CO_2R. Besides this, the PZC can be also modified by altering the surface composition. Previous studies electrodeposited a Ag monolayer on Pt or Au and found the PZC to be up to 0.25 V more positive compared to Ag(111). Moreover, a recent study that

deposited Au nanoparticles with a highly positive PZC on a Cu electrode has found increased C_2 selectivity[129] that we suggest to be also likely attributed to the more positive PZC compared to Cu. We anticipate that the outlined strategies are fully generalizable to other field-sensitive electrochemical processes, highlighting their significant impact on the electrocatalyst design.

CONCLUSIONS

In this work, we developed a combined ab initio/continuum model of cation and electric double layer field effects in electrocatalysis that was validated against a wide range of experimental data. With the continuum, modified Poisson Boltzmann approach we find that the surface charge density and the associated electric field are essentially altered by repulsive interactions amongst hydrated cations in the Helmholtz layer. This effect, combined with surface-charge dependent reaction energetics determined using DFT, allowed for the theoretical prediction of ion-specific catalytic activities.

Using a single set of cation sizes derived from experimental data, the model showed quantitative agreement with experimentally observed cation effects on CO production on Ag, and C_2 production on Cu, as well as the respective surface facet dependence. The model also correctly predicted cation effects on the vibrational stretching mode of *CO on Pt and Cu, as well as on the double layer capacitance of Au(111) single crystal electrodes determined by impedance spectroscopy.

The unprecedented agreement with diverse experimental data sets demonstrated the generality of the developed understanding of cation and field effects. Finally, we present some universal design principles to optimize the conversion efficiency of field-sensitive electrochemical processes. These comprise the use of high valent cations with a small hydration radius, but also the increase of the potential of zero charge or capacitance in order to maximize surface charge density the corresponding interfacial electric fields. These general design principles represent a major step forward for solid-liquid interface engineering for electrocatalysis.

EXPERIMENTAL

Electrode Preparation

Cu and Ag thin films were deposited onto polished single crystal Si wafers (1-10 Ω·cm Virginia Semiconductor) with (111), (100), and (110) orientations using an AJA ATC Orion-5 magnetron sputtering system. The Si wafers were etched immediately before deposition using 5 wt. % HF. Cu thin films were deposited at room temperature and Ag thin films were deposited at 300 °C using an IR lamp. Cu (99.999% Kurt J. Lesker) and Ag (99.999% Kurt J. Lesker) were sputtered using Ar ions onto the etched Si wafers at a rate of 1 Å/s to obtain a thin film with a thickness of 100 nm.

Electrode Characterization

The crystal structures of the Cu and Ag thin films were analyzed with a Rigaku Smartlab x-ray diffractometer (XRD) using Cu Kα radiation (40 kV, 40 mA). Symmetric out-of-plane $\theta/2\theta$ scans were conducted to identify the out-of-plane growth orientation of the crystallites in the thin films. Symmetric in-plane φ scans at Bragg reflections corresponding to both Si and the metallic thin film were conducted to determine the orientation of the thin film crystallites with respect to the Si substrate. Symmetric out-of-plane Ω scans were conducted to determine the average degree of misorientation of the thin film crystallites with respect to the surface normal. X-ray pole figures of the thin films were acquired using a PANanalytical X'Pert diffractometer using Cu Kα radiation. The near-surface composition of the thin films was measured before and after electrolysis with a Kratos Axis Ultra DLD x-ray photoelectron spectrometer (XPS). All spectra were acquired using monochromatized Al Kα radiation (15 kV, 15 mA). The kinetic energy scale of the measured spectra was calibrated by setting the C 1s binding energy to 284.8 eV. The same instrument was also used to measure the surface composition of the thin films before and after electrolysis by ion scattering spectroscopy (ISS).

Electrochemical Characterization

All electrochemical activity measurements were conducted in a custom gas-tight electrochemical cell machined from PEEK.1 The cell was sonicated in 20 wt. % nitric acid and thoroughly rinsed with DI water prior to all experimentation. The working and counter electrodes were parallel and separated by an anion exchange membrane (Selemion AMV AGC Inc.). Gas dispersion frits were incorporated into both electrode chambers to provide ample electrolyte mixing. The exposed geometric surface area of each electrode was 1 cm^2 and the electrolyte volume of each electrode chamber was 1.8 mL. The counter electrode was a glassy carbon plate (Type 2 Alfa Aesar) that was also sonicated in 20 wt. % nitric acid prior to all experimentation. Platinum was not used as the anode due to the possibility of contaminating the cathode.[31,130] The working electrode potential was referenced against a miniature Ag/AgCl electrode (Innovative Instruments Inc.) that was calibrated against a homemade standard hydrogen electrode. 0.05 M M_2CO_3 (M = Li, Na, K, and Cs 99.995% Sigma Aldrich) solutions prepared using 18.2 MΩ·cm DI water were used as the electrolyte. Metallic impurities in the as-prepared electrolytes were removed before electrolysis by chelating them with Chelex 100 (Na form Sigma Aldrich) except

in the case of Li, which was not purified by additional means.[130,131] Both electrode chambers were sparged with CO_2 (99.999% Praxair Inc.) at a rate of 10 sccm for 30 min prior to and throughout the duration of all electrochemical measurements unless explicitly stated otherwise. Upon saturation with CO_2 the pH of the electrolyte was 6.8, which was maintained throughout the duration of all electrocatalytic measurements. The hydrodynamic boundary layer thickness at the cathode surface was determined to be 50 μm by measuring the diffusion limited current of ferricyanide reduction.

Double layer capacitance measurements were performed in a glass cell that was cleaned with aqua regia prior to all experimentation. The working electrode was a Au(111) single crystal that was annealed prior to each measurement and utilized in the hanging meniscus configuration. The counter electrode was a Au wire and the reference electrode was a Ag/AgCl electrode (Pine Research). 0.05 M $MClO_4$ (M = Na and K 99.99% Sigma Aldrich) solutions prepared using 18.2 MΩ·cm DI water were used as the electrolyte. Metallic impurities in the as-prepared electrolytes were removed before electrolysis by chelating them with Chelex 100 (Na form Sigma Aldrich).[130,131] The electrolyte was sparged with Ar (99.999% Praxair Inc.) for 30 min prior to all electrochemical measurements. The headspace of the electrochemical cell was swept with Ar during all measurements to prevent oxygenation while minimizing measurement artifacts arising from electrolyte agitation.

Electrochemistry was performed using a Biologic VSP-300 potentiostat. All electrochemical measurements were recorded versus the reference electrode and converted to the RHE scale. Potentiostatic electrochemical impedance spectroscopy (PEIS) was used to determine the uncompensated resistance (Ru) of the electrochemical cell and the double layer capacitance (C_{dl}) by applying voltage waveforms with an amplitude of 20 mV and frequencies ranging from 5 Hz to 500 kHz. The potentiostat compensated for 85 % of R_u *in-situ* and the last 15 % was post-corrected to arrive at accurate potentials. The electrocatalytic activity of the thin films was assessed by conducting chronoamperometry staircases from -0.5 to -1.5 V vs RHE with a step size of 100 mV and a step length of 15 min. Each thin film orientation was tested at least three separate times to ensure the statistical relevance of the observed trends.

A. Product Analysis

The effluent from the electrochemical cell was introduced directly into the sampling loop of an Agilent 7890B gas chromatograph (GC) equipped with a pulsed-discharge helium ionization detector (PDHID). The effluent was sampled at least 10 min after each chronoamperometry potential step. The constituents of the gaseous sample were separated using a Hayesep-Q capillary column (Agilent) in series with a packed ShinCarbon ST column (Restek Co.). He (99.9999 % Praxair Inc.) was used as the carrier gas. After sampling the effluent of the electrochemical cell, the column oven was maintained at 50 for 1 min followed by a temperature ramp at 30 °C/min to 250 °C, which was then maintained for the duration of the analysis. The signal response of the PDHID was calibrated by analyzing a series of NIST-traceable standard gas mixtures (Airgas Inc.).

The electrolyte from both electrode chambers was collected after electrolysis and analyzed using a Thermo Scientific UltiMate 3000 liquid chromatograph (HPLC) equipped with a refractive index detector (RID). The electrolyte samples were stored in a refrigerated autosampler until analyzed to minimize the evaporation of volatile liquid-phase reaction products. The liquid-phase products contained in a 10 μL aliquot were separated using a series of two Aminex HPX 87-H columns (Bio-Rad Inc.) and a 1 mM sulfuric acid eluent (99.999 % Sigma Aldrich). The column oven was maintained at 60 °C for the duration of the analysis. The signal response of the RID was calibrated by analyzing standard solutions of each product at a concentration of 1, 10, and 50 mM (see SI-6).

CONFLICTS OF INTEREST

There are no conflicts of interest to declare.

ACKNOWLEDGMENTS

This material is based in part on work performed by the Joint Center for Artificial Photosynthesis, a DOE Energy Innovation Hub, supported through the Office of Science of the U.S. Department of Energy, under Award No. DE-SC0004993. This research used resources of the National Energy Research Scientific Computing Center, a DOE Office of Science User Facility supported by the Office of Science of the U.S. Department of Energy under Contract No. DE-AC02-05CH11231. I.C., B.S., and K.C. also acknowledge a research grant (9455) from "VILLUM FONDEN". We also thank Bingjun Xu and Aliaksandr Bandarenka for insightful discussions.

[1] Lu, Q.; Jiao, F. Electrochemical CO2 reduction: Electrocatalyst, reaction mechanism, and process engineering. *Nano Energy* **2016**, *29*, 439–456.

[2] Liu, M. et al. Enhanced electrocatalytic CO2 reduction via field-induced reagent concentration. *Nature* **2016**, *537*, 382–386.

[3] Sandberg, R. B.; Montoya, J. H.; Chan, K.; Nørskov, J. K. CO-CO coupling on Cu facets: Coverage, strain and field effects. *Surf. Sci.* **2016**, *654*, 56–62.

[4] Resasco, J.; Chen, L. D.; Clark, E.; Tsai, C.; Hahn, C.; Jaramillo, T. F.; Chan, K.; Bell, A. T. Promoter Effects of Alkali Metal Cations on the Electrochemical Reduction of Carbon Dioxide. *J. Am. Chem. Soc.* **2017**, *139*, 11277–11287.

[5] Clark, E. L.; Ringe, S.; Tang, M.; Walton, A. L.; Hahn, C.; Jaramillo, T. F.; Chan, K.; Bell, A. T. Influence of Atomic Surface Structure on the Activity of Ag for the Electrochemical Reduction of CO2 to CO. *ACS Catal.* **2019**,

[6]Gauthier, J. A.; Ringe, S.; Dickens, C. F.; Garza, A. J.; Bell, A. T.; Head-Gordon, M.; Nørskov, J. K.; Chan, K. Challenges in Modeling Electrochemical Reaction Energetics with Polarizable Continuum Models. *ACS Catal.* **2019**, *9*, 920–931.

[7]Liu, X.; Schlexer, P.; Xiao, J.; Ji, Y.; Wang, L.; Sandberg, R. B.; Tang, M.; Brown, K. S.; Peng, H.; Ringe, S.; Hahn, C.; Jaramillo, T. F.; Nørskov, J. K.; Chan, K. pH effects on the electrochemical reduction of CO(2) towards C2 products on stepped copper. *Nat. Commun.* **2019**, *10*, 32.

[8]Katsounaros, I.; Meier, J. C.; Klemm, S. O.; Topalov, A. A.; others, The effective surface pH during reactions at the solid-liquid interface. *Electrochemistry* **2011**,

[9]Ledezma-Yanez, I.; Wallace, W. D. Z.; Sebastián-Pascual, P.; Climent, V.; Feliu, J. M.; Koper, M. T. M. Interfacial water reorganization as a pH-dependent descriptor of the hydrogen evolution rate on platinum electrodes. *Nature Energy* **2017**, *2*, 17031.

[10]Giordano, L.; Han, B.; Risch, M.; Hong, W. T.; Rao, R. R.; Stoerzinger, K. A.; Shao-Horn, Y. pH dependence of OER activity of oxides: Current and future perspectives. *Catal. Today* **2016**, *262*, 2–10.

[11]Xiao, H.; Cheng, T.; Goddard, W. A., 3rd; Sundararaman, R. Mechanistic Explanation of the pH Dependence and Onset Potentials for Hydrocarbon Products from Electrochemical Reduction of CO on Cu (111). *J. Am. Chem. Soc.* **2016**, *138*, 483–486.

[12]Singh, M. R.; Goodpaster, J. D.; Weber, A. Z.; Head-Gordon, M.; Bell, A. T. Mechanistic insights into electrochemical reduction of CO2 over Ag using density functional theory and transport models. *Proc. Natl. Acad. Sci. U. S. A.* **2017**, *114*, E8812–E8821.

[13]Gupta, N.; Gattrell, M.; MacDougall, B. Calculation for the cathode surface concentrations in the electrochemical reduction of CO2 in KHCO3 solutions. *J. Appl. Electrochem.* **2006**, *36*, 161–172.

[14]Dunwell, M.; Yang, X.; Setzler, B. P.; Anibal, J.; Yan, Y.; Xu, B. Examination of Near-Electrode Concentration Gradients and Kinetic Impacts on the Electrochemical Reduction of CO2 using Surface-Enhanced Infrared Spectroscopy. *ACS Catal.* **2018**, 3999–4008.

[15]Suter, S.; Haussener, S. Optimizing Mesostructured Silver Catalysts for Selective Carbon Dioxide Conversion into Fuels. *Energy Environ. Sci.* **2019**,

[16]Burdyny, T.; Smith, W. A. CO2 reduction on gas-diffusion electrodes and why catalytic performance must be assessed at commercially-relevant conditions. *Energy Environ. Sci.* **2019**,

[17]Benn, E. E.; Gaskey, B.; Erlebacher, J. D. Suppression of Hydrogen Evolution by Oxygen Reduction in Nanoporous Electrocatalysts. *J. Am. Chem. Soc.* **2017**, *139*, 3663–3668.

[18]Verdaguer-Casadevall, A.; Li, C. W.; Johansson, T. P.; Scott, S. B.; McKeown, J. T.; Kumar, M.; Stephens, I. E. L.; Kanan, M. W.; Chorkendorff, I. Probing the Active Surface Sites for CO Reduction on Oxide-Derived Copper Electrocatalysts. *J. Am. Chem. Soc.* **2015**, *137*, 9808–9811.

[19]Gao, D.; McCrum, I. T.; Deo, S.; Choi, Y.-W.; Scholten, F.; Wan, W.; Chen, J. G.; Janik, M. J.; Roldan Cuenya, B. Activity and Selectivity Control in CO2 Electroreduction to Multicarbon Products over CuOx Catalysts via Electrolyte Design. *ACS Catal.* **2018**, 10012–10020.

[20]Lu, Q.; Rosen, J.; Zhou, Y.; Hutchings, G. S.; Kimmel, Y. C.; Chen, J. G.; Jiao, F. A selective and efficient electrocatalyst for carbon dioxide reduction. *Nat. Commun.* **2014**, *5*, 3242.

[21]Rosen, J.; Hutchings, G. S.; Lu, Q.; Rivera, S.; Zhou, Y.; Vlachos, D. G.; Jiao, F. Mechanistic Insights into the Electrochemical Reduction of CO2 to CO on Nanostructured Ag Surfaces. *ACS Catal.* **2015**, *5*, 4293–4299.

[22]Mistry, H.; Choi, Y.-W.; Bagger, A.; Scholten, F.; Bonifacio, C. S.; Sinev, I.; Divins, N. J.; Zegkinoglou, I.; Jeon, H. S.; Kisslinger, K.; Stach, E. A.; Yang, J. C.; Rossmeisl, J.; Roldan Cuenya, B. Enhanced Carbon Dioxide Electroreduction to Carbon Monoxide over Defect-Rich Plasma-Activated Silver Catalysts. *Angew. Chem. Int. Ed.* **2017**, *56*, 11394–11398.

[23]Roberts, F. S.; Kuhl, K. P.; Nilsson, A. High Selectivity for Ethylene from Carbon Dioxide Reduction over Copper Nanocube Electrocatalysts. *Angew. Chem. Int. Ed.* **2015**, *54*, 5179–5182.

[24]Eilert, A.; Roberts, F. S.; Friebel, D.; Nilsson, A. Formation of Copper Catalysts for CO2 Reduction with High Ethylene/Methane Product Ratio Investigated with In Situ X-ray Absorption Spectroscopy. *J. Phys. Chem. Lett.* **2016**, *7*, 1466–1470.

[25]Lu, Q.; Rosen, J.; Jiao, F. Nanostructured Metallic Electrocatalysts for Carbon Dioxide Reduction. *Chem. Cat. Chem.* **2015**, *7*, 38–47.

[26]Mellmer, M. A.; Sanpitakseree, C.; Demir, B.; Bai, P.; Ma, K.; Neurock, M.; Dumesic, J. A. Solvent-enabled control of reactivity for liquid-phase reactions of biomass-derived compounds. *Nature Catalysis* **2018**, *1*, 199.

[27]Zhao, Z.; Bababrik, R.; Xue, W.; Li, Y.; Briggs, N. M.; Nguyen, D.-T.; Nguyen, U.; Crossley, S. P.; Wang, S.; Wang, B.; Resasco, D. E. Solvent-mediated charge separation drives alternative hydrogenation path of furanics in liquid water. *Nature Catalysis* **2019**, 1.

[28]Lim, H.-K.; Kwon, Y.; Kim, H. S.; Jeon, J.; Kim, Y.-H.; Lim, J.-A.; Kim, B.-S.; Choi, J.; Kim, H. Insight into the Microenvironments of the Metal-Ionic Liquid Interface during Electrochemical CO2 Reduction. *ACS Catal.* **2018**, *8*, 2420–2427.

[29]Yang, K.; Kas, R.; Smith, W. A. Tenacious Mass Transfer Limitations Drive Catalytic Selectivity during Electrochemical Carbon Dioxide Reduction. **2019**,

[30]Varela, A. S.; Kroschel, M.; Reier, T.; Strasser, P. Controlling the selectivity of CO2 electroreduction on copper: The effect of the electrolyte concentration and the importance of the local pH. *Catal. Today* **2016**, *260*, 8–13.

[31]Dunwell, M.; Lu, Q.; Heyes, J. M.; Rosen, J.; Chen, J. G.; Yan, Y.; Jiao, F.; Xu, B. The Central Role of Bicarbonate in the Electrochemical Reduction of Carbon Dioxide on Gold. *J. Am. Chem. Soc.* **2017**, *139*, 3774–3783.

[32]Resasco, J.; Lum, Y.; Clark, E.; Zeledon, J. Z.; Bell, A. T. Effects of Anion Identity and Concentration on Electrochemical Reduction of CO 2. *ChemElectroChem* **2018**, *5*, 1064–1072.

[33]García, G.; Stoffelsma, C.; Rodriguez, P.; Koper, M. T. M. Influence of beryllium cations on the electrochemical oxidation of methanol on stepped platinum surfaces in alkaline solution. *Surf. Sci.* **2015**, *631*, 267–271.

[34]McDonnell-Worth, C.; MacFarlane, D. R. Ion effects in water oxidation to hydrogen peroxide. *RSC Adv.* **2014**, *4*, 30551–30557.

[35]Stoffelsma, C.; Rodriguez, P.; Garcia, G.; Garcia-Araez, N.; Strmcnik, D.; Marković, N. M.; Koper, M. T. M. Promotion of the oxidation of carbon monoxide at stepped platinum single-crystal electrodes in alkaline media by lithium and beryllium cations. *J. Am. Chem. Soc.* **2010**, *132*, 16127–16133.

[36]Previdello, B. A. F.; Machado, E. G.; Varela, H. The effect of the alkali metal cation on the electrocatalytic oxidation of formate on platinum. *RSC Adv.* **2014**, *4*, 15271–15275.

[37]Ragoisha, G. A.; Auchynnikava, T. A.; Streltsov, E. A.; Rabchynski, S. M. Electrochemical impedance of platinum in concentrated chloride solutions under potentiodynamic anodic polarization: Effect of alkali metal cations. *Electrochim. Acta* **2014**, *122*, 218–223.

[38]Strmcnik, D.; Kodama, K.; van der Vliet, D.; Greeley, J.; Stamenkovic, V. R.; Marković, N. M. The role of non-covalent interactions in electrocatalytic fuel-cell reactions on platinum. *Nat. Chem.* **2009**, *1*, 466–472.

[39]Strmcnik, D.; van der Vliet, D. F.; Chang, K.-C.; Komanicky, V.; Kodama, K.; You, H.; Stamenkovic, V. R.; Marković, N. M. Effects of Li+, K+, and Ba2+ Cations on the ORR at Model and High Surface Area Pt and Au Surfaces in Alkaline Solutions. *J. Phys. Chem. Lett.* **2011**, *2*, 2733–2736.

[40]Frumkin, A. N. Influence of cation adsorption on the kinetics of electrode processes. *Trans. Faraday Soc.* **1959**, *55*, 156–167.

[41]Murata, A.; Hori, Y. Product Selectivity Affected by Cationic Species in Electrochemical Reduction of CO2 and CO at a Cu Electrode. *BCSJ* **1991**, *64*, 123–127.
[42]Paik, W.; Andersen, T. N.; Eyring, H. Kinetic studies of the electrolytic reduction of carbon dioxide on the mercury electrode. *Electrochim. Acta* **1969**, *14*, 1217–1232.
[43]Kaneco, S.; Iiba, K.; Katsumata, H.; Suzuki, T.; Ohta, K. Effect of sodium cation on the electrochemical reduction of CO2 at a copper electrode in methanol. *J. Solid State Electrochem.* **2007**, *11*, 490–495.
[44]Thorson, M. R.; Siil, K. I.; Kenis, P. J. A. Effect of Cations on the Electrochemical Conversion of CO2 to CO. *J. Electrochem. Soc.* **2013**, *160*, F69–F74.
[45]Singh, M. R.; Kwon, Y.; Lum, Y.; Ager, J. W., 3rd; Bell, A. T. Hydrolysis of Electrolyte Cations Enhances the Electrochemical Reduction of CO2 over Ag and Cu. *J. Am. Chem. Soc.* **2016**, *138*, 13006–13012.
[46]Pérez-Gallent, E.; Marcandalli, G.; Figueiredo, M. C.; Calle-Vallejo, F.; Koper, M. T. M. Structure- and Potential-Dependent Cation Effects on CO Reduction at Copper Single-Crystal Electrodes. *J. Am. Chem. Soc.* **2017**, *139*, 16412–16419.
[47]Sitta, E.; Batista, B. C.; Varela, H. The impact of the alkali cation on the mechanism of the electro-oxidation of ethylene glycol on Pt. *Chem. Commun.* **2011**, *47*, 3775–3777.
[48]Suntivich, J.; Perry, E. E.; Gasteiger, H. A.; Shao-Horn, Y. The Influence of the Cation on the Oxygen Reduction and Evolution Activities of Oxide Surfaces in Alkaline Electrolyte. *Electrocatalysis* **2013**, *4*, 49–55.
[49]Zhu, S.; Hu, X.; Zhang, L.; Shao, M. Impacts of Perchloric Acid, Nafion, and Alkali Metal Ions on Oxygen Reduction Reaction Kinetics in Acidic and Alkaline Solutions. *J. Phys. Chem. C* **2016**, *120*, 27452–27461.
[50]Pérez-Gallent, E.; Marcandalli, G.; Figueiredo, M. C.; Calle-Vallejo, F.; Koper, M. T. M. Structure- and Potential-Dependent Cation Effects on CO Reduction at Copper Single-Crystal Electrodes. *Journal of the American Chemical Society* **2017**, *139*, 16412–16419, PMID: 29064691.
[51]Akhade, S. A.; McCrum, I. T.; Janik, M. J. The Impact of Specifically Adsorbed Ions on the Copper-Catalyzed Electroreduction of CO2. *Journal of The Electrochemical Society* **2016**, *163*, F477–F484.
[52]Vanysek, P. In *CRC Handbook of Chemistry and Physics*; Lide, D. R., Ed.; CRC Press LLC, pp 8–23.
[53]Stern, O. Theory of the electrolytic double layer. *Z. Elektrochem. Angew. Phys. Chem.* **1924**, *30*, 508–516.
[54]Chapman, D. L. Theory of electrocapillarity. *Philos. Mag.* **1913**, *25*, 475–481.
[55]Gouy, G. Constitution of the electric charge at the surface of an electrolyte. *J. de Physique* **1910**, *9*, 457–468.
[56]Borukhov, I.; Andelman, D.; Orland, H. Adsorption of large ions from an electrolyte solution: a modified Poisson-Boltzmann equation. *Electrochim. Acta* **2000**, *46*, 221–229.
[57]Chen, L. D.; Urushihara, M.; Chan, K.; Nørskov, J. K. Electric Field Effects in Electrochemical CO2 Reduction. *ACS Catal.* **2016**, *6*, 7133–7139.
[58]Andreussi, O.; Dabo, I.; Marzari, N. Revised self-consistent continuum solvation in electronic-structure calculations. *J. Chem. Phys.* **2012**, *136*, 064102.
[59]Sundararaman, R.; Schwarz, K. Evaluating continuum solvation models for the electrode-electrolyte interface: Challenges and strategies for improvement. *J. Chem. Phys.* **2017**, *146*, 084111.
[60]Nattino, F.; Truscott, M.; Marzari, N.; Andreussi, O. Continuum models of the electrochemical diffuse layer in electronic-structure calculations. **2019**, 041722.
[61]Jinnouchi, R.; Anderson, A. B. Electronic structure calculations of liquid-solid interfaces: Combination of density functional theory and modified Poisson-Boltzmann theory. *Phys. Rev. B Condens. Matter* **2008**, *77*, 245417.
[62]Ringe, S.; Oberhofer, H.; Hille, C.; Matera, S.; Reuter, K. Function-Space-Based Solution Scheme for the Size-Modified Poisson-Boltzmann Equation in Full-Potential DFT. *J. Chem. Theory Comput.* **2016**, *12*, 4052–4066.
[63]Ringe, S.; Oberhofer, H.; Reuter, K. Transferable ionic parameters for first-principles Poisson-Boltzmann solvation calculations: Neutral solutes in aqueous monovalent salt solutions. *J. Chem. Phys.* **2017**, *146*, 134103.
[64]Letchworth-Weaver, K.; Arias, T. A. Joint density functional theory of the electrode-electrolyte interface: Application to fixed electrode potentials, interfacial capacitances, and potentials of zero charge. *Phys. Rev. B Condens. Matter* **2012**, *86*, 075140.
[65]Hörmann, N. G.; Andreussi, O.; Marzari, N. Grand canonical simulations of electrochemical interfaces in implicit solvation models. *J. Chem. Phys.* **2019**, *150*, 041730.
[66]Fang, Y.-H.; Wei, G.-F.; Liu, Z.-P. Theoretical modeling of electrode/electrolyte interface from first-principles periodic continuum solvation method. *Catal. Today* **2013**, *202*, 98–104.
[67]Mathew, K.; Hennig, R. G. Implicit self-consistent description of electrolyte in plane-wave density-functional theory. **2016**,
[68]Otani, M.; Sugino, O. First-principles calculations of charged surfaces and interfaces: A plane-wave nonrepeated slab approach. *Phys. Rev. B Condens. Matter* **2006**, *73*, 115407.
[69]Dabo, I.; Li, Y.; Bonnet, N.; Marzari, N. In *Fuel Cell Science*; Wieckowski, A., Nørskov, J. K., Eds.; Electrodics 2A; John Wiley & Sons, Inc.: Hoboken, NJ, USA, 2010; Vol. 10; pp 415–431.
[70]Sundararaman, R.; Letchworth-Weaver, K.; Schwarz, K. A. Improving accuracy of electrochemical capacitance and solvation energetics in first-principles calculations. *J. Chem. Phys.* **2018**, *148*, 144105.
[71]Gomer, R.; Tryson, G. An experimental determination of absolute half-cell emf's and single ion free energies of solvation. *J. Chem. Phys.* **1977**, *66*, 4413–4424.
[72]Kötz, E. R.; Neff, H.; Müller, K. A UPS, XPS and work function study of emersed silver, platinum and gold electrodes. *J. Electroanal. Chem. Interfacial Electrochem.* **1986**, *215*, 331–344.
[73]Hansen, W. N.; Hansen, G. J. Absolute half-cell potential: A simple direct measurement. *Phys. Rev. A Gen. Phys.* **1987**, *36*, 1396–1402.
[74]Fawcett, W. R. The ionic work function and its role in estimating absolute electrode potentials. *Langmuir* **2008**, *24*, 9868–9875.
[75]Isse, A. A.; Gennaro, A. Absolute potential of the standard hydrogen electrode and the problem of interconversion of potentials in different solvents. *J. Phys. Chem. B* **2010**, *114*, 7894–7899.
[76]Haruyama, J.; Ikeshoji, T.; Otani, M. Electrode potential from density functional theory calculations combined with implicit solvation theory. *Phys. Rev. Materials* **2018**, *2*, 095801.
[77]Lucas, C. A.; Thompson, P.; Gründer, Y.; Markovic, N. M. The structure of the electrochemical double layer: Ag(111) in alkaline electrolyte. *Electrochem. commun.* **2011**, *13*, 1205–1208.
[78]Nakamura, M.; Sato, N.; Hoshi, N.; Sakata, O. Outer Helmholtz plane of the electrical double layer formed at the solid electrode-liquid interface. *Chemphyschem* **2011**, *12*, 1430–1434.
[79]Nakamura, M.; Nakajima, Y.; Hoshi, N.; Tajiri, H.; Sakata, O. Effect of Non-Specifically Adsorbed Ions on the Surface Oxidation of Pt(111). *Chemphyschem* **2013**, *14*, 2426–2431.
[80]Nakamura, M.; Kaminaga, H.; Endo, O.; Tajiri, H.; Sakata, O.; Hoshi, N. Structural Dynamics of the Electrical Double Layer during Capacitive Charging/Discharging Processes. *J. Phys. Chem. C* **2014**, *118*, 22136–22140.
[81]Nakamura, M.; Nakajima, Y.; Kato, K.; Sakata, O.; Hoshi, N. Surface Oxidation of Au(111) Electrode in Alkaline Media Studied by Using X-ray Diffraction and Infrared Spectroscopy: Effect of Alkali Metal Cation on the Alcohol Oxidation Reactions. *J. Phys. Chem. C* **2015**, *119*, 23586–23591.
[82]Nightingale, E. R. Phenomenological Theory of Ion Solvation. Effective Radii of Hydrated Ions. *J. Phys. Chem.* **1959**, *63*, 1381–1387.
[83]Chan, K.; Eikerling, M. A Pore-Scale Model of Oxygen Reduction in Ionomer-Free Catalyst Layers of PEFCs. *J. Electrochem.*

Soc. **2011**, *158*, B18–B28.

[84]Huang, J.; Malek, A.; Zhang, J.; Eikerling, M. H. Non-monotonic Surface Charging Behavior of Platinum: A Paradigm Change. *J. Phys. Chem. C* **2016**, *120*, 13587–13595.

[85]Ando, Y.; Gohda, Y.; Tsuneyuki, S. Ab initio molecular dynamics study of the Helmholtz layer formed on solid-liquid interfaces and its capacitance. *Chem. Phys. Lett.* **2013**, *556*, 9–12.

[86]Ruzanov, A.; Karu, K.; Ivaništšev, V.; Nazmutdinov, R. R.; Lust, E. Interplay between the hydrophilicity of metal electrodes and their interfacial capacitance. *Electrochim. Acta* **2016**, *210*, 615–621.

[87]Sundararaman, R.; Figueiredo, M. C.; Koper, M. T. M.; Schwarz, K. A. Electrochemical Capacitance of CO-Terminated Pt(111) Dominated by the CO-Solvent Gap. *J. Phys. Chem. Lett.* **2017**, *8*, 5344–5348.

[88]Hamelin, A.; Vitanov, T.; Sevastyanov, E.; Popov, A. The electrochemical double layer on sp metal single crystals: The current status of data. *J. Electroanal. Chem. Interfacial Electrochem.* **1983**, *145*, 225–264.

[89]Kornyshev, A. A.; Spohr, E.; Vorotyntse, M. A. In *Encyclopedia of Electrochemistry*; Bard, A. J., Ed.; Techn. Report no 14 to the office of Naval Research of Febr. 18, 1954; Wiley-VCH Verlag GmbH & Co. KGaA: Weinheim, Germany, 2007; Vol. 41; p 2307.

[90]Lust, E. In *Encyclopedia of Electrochemistry*; Bard, A. J., Ed.; Wiley-VCH Verlag GmbH & Co. KGaA: Weinheim, Germany, 2007; Vol. 16; p 1.

[91]Valette, G. Double layer on silver single-crystal electrodes in contact with electrolytes having anions which present a slight specific adsorption: Part I. The (110) face. *J. Electroanal. Chem. Interfacial Electrochem.* **1981**, *122*, 285–297.

[92]Valette, G. Double layer on silver single crystal electrodes in contact with electrolytes having anions which are slightly specifically adsorbed: Part II. The (100) face. *J. Electroanal. Chem. Interfacial Electrochem.* **1982**, *138*, 37–54.

[93]Valette, G. Double layer on silver single crystal electrodes in contact with electrolytes having anions which are slightly specifically adsorbed: Part III. The (111) face. *J. Electroanal. Chem. Interfacial Electrochem.* **1989**, *269*, 191–203.

[94]Weidenauer, M.; Weil, K. G. Studies of the Differential Double Layer Capacitance of the Copper (111) Face in Aqueous Solutions. *Berichte der Bunsengesellschaft für physikalische Chemie* **1988**, *92*, 1368–1372.

[95]Pajkossy, T.; Kolb, D. M. On the origin of the double layer capacitance maximum of Pt(111) single crystal electrodes. *Electrochem. commun.* **2003**, *5*, 283–285.

[96]Rossmeisl, J.; Skúlason, E.; Björketun, M. E.; Tripkovic, V.; Nørskov, J. K. Modeling the electrified solid–liquid interface. *Chem. Phys. Lett.* **2008**, *466*, 68–71.

[97]Chan, K.; Nørskov, J. K. Electrochemical Barriers Made Simple. *J. Phys. Chem. Lett.* **2015**, *6*, 2663–2668.

[98]Weitzner, S. E.; Dabo, I. Voltage-dependent cluster expansion for electrified solid-liquid interfaces: Application to the electrochemical deposition of transition metals. *Phys. Rev. B Condens. Matter* **2017**, *96*, 205134.

[99]Rosen, B. A.; Salehi-Khojin, A.; Thorson, M. R.; Zhu, W.; Whipple, D. T.; Kenis, P. J. A.; Masel, R. I. Ionic liquid-mediated selective conversion of CO2 to CO at low overpotentials. *Science* **2011**, *334*, 643–644.

[100]Wuttig, A.; Yoon, Y.; Ryu, J.; Surendranath, Y. Bicarbonate Is Not a General Acid in Au-Catalyzed CO2 Electroreduction. *J. Am. Chem. Soc.* **2017**,

[101]Wuttig, A.; Yaguchi, M.; Motobayashi, K.; Osawa, M.; Surendranath, Y. Inhibited proton transfer enhances Au-catalyzed CO2-to-fuels selectivity. *Proc. Natl. Acad. Sci. U. S. A.* **2016**, *113*, E4585–93.

[102]Dunwell, M.; Luc, W.; Yan, Y.; Jiao, F.; Xu, B. Understanding Surface-Mediated Electrochemical Reactions: CO2 Reduction and Beyond. *ACS Catal.* **2018**, *8*, 8121–8129.

[103]Firet, N. J.; Smith, W. A. Probing the Reaction Mechanism of CO2 Electroreduction over Ag Films via Operando Infrared Spectroscopy. *ACS Catal.* **2017**, *7*, 606–612.

[104]Chernyshova, I. V.; Somasundaran, P.; Ponnurangam, S. On the origin of the elusive first intermediate of CO2 electroreduction. *Proc. Natl. Acad. Sci. U. S. A.* **2018**,

[105]Michal Bajdich, Meredith Fields, Leanne D. Chen, Robert B. Sandberg, Karen Chan,Jens K. Nørskov, Electron Transfer to CO2 during Adsorption at the Metal — Solution Interface. *J. Phys. Chem. Lett.*

[106]Cheng, T.; Xiao, H.; Goddard, W. A., 3rd Full atomistic reaction mechanism with kinetics for CO reduction on Cu(100) from ab initio molecular dynamics free-energy calculations at 298 K. *Proc. Natl. Acad. Sci. U. S. A.* **2017**, *114*, 1795–1800.

[107]Huang, Y.; Handoko, A. D.; Hirunsit, P.; Yeo, B. S. Electrochemical Reduction of CO2 Using Copper Single-Crystal Surfaces: Effects of CO* Coverage on the Selective Formation of Ethylene. *ACS Catal.* **2017**, *7*, 1749–1756.

[108]Tsang, C. F.; Javier, A. C.; Kim, Y.-G.; Baricuatro, J. H.; Cummins, K. D.; Kim, J.; Jerkiewicz, G.; Hemminger, J. C.; Soriaga, M. P. Potential-Dependent Adsorption of CO and Its Low-Overpotential Reduction to CH3CH2OH on Cu(511) Surface Reconstructed from Cu(pc): Operando Studies by Seriatim STM-EQCN-DEMS. *J. Electrochem. Soc.* **2018**, *165*, J3350–J3354.

[109]Trasatti, S.; Lust, E. *Modern aspects of electrochemistry*; Springer, 2002; pp 1–215.

[110]Cuesta, A. Measurement of the surface charge density of CO-saturated Pt(111) electrodes as a function of potential: the potential of zero charge of Pt(111). *Surf. Sci.* **2004**, *572*, 11–22.

[111]Mezzavilla, S.; Horch, S.; Stephens, I. E. L.; Seger, B.; Chorkendorff, I. Structure Sensitivity in the Electrocatalytic Reduction of CO2 with Gold Catalysts. *Angew. Chem. Int. Ed Engl.* **2019**,

[112]Anderson, M. R.; Huang, J. The influence of cation size upon the infrared spectrum of carbon monoxide adsorbed on platinum electrodes. *J. Electroanal. Chem. Interfacial Electrochem.* **1991**, *318*, 335–347.

[113]Tao, F.; Dag, S.; Wang, L.-W.; Liu, Z.; Butcher, D. R.; Bluhm, H.; Salmeron, M.; Somorjai, G. A. Break-up of stepped platinum catalyst surfaces by high CO coverage. *Science* **2010**, *327*, 850–853.

[114]Grinberg, I.; Yourdshahyan, Y.; Rappe, A. M. CO on Pt(111) puzzle: A possible solution. *J. Chem. Phys.* **2002**, *117*, 2264–2270.

[115]Mamatkulov, M.; Filhol, J.-S. An ab initio study of electrochemical vs. electromechanical properties: the case of CO adsorbed on a Pt(111) surface. *Phys. Chem. Chem. Phys.* **2011**, *13*, 7675–7684.

[116]Farias, M. J. S.; Herrero, E.; Feliu, J. M. Site Selectivity for CO Adsorption and Stripping on Stepped and Kinked Platinum Surfaces in Alkaline Medium. *J. Phys. Chem. C* **2013**, *117*, 2903–2913.

[117]Dimakis, N.; Navarro, N. E.; Mion, T.; Smotkin, E. S. Carbon Monoxide Adsorption Coverage Study on Platinum and Ruthenium Surfaces. *J. Phys. Chem. C* **2014**, *118*, 11711–11722.

[118]Gunathunge, C. M.; Ovalle, V. J.; Waegele, M. M. Probing promoting effects of alkali cations on the reduction of CO at the aqueous electrolyte/copper interface. *Phys. Chem. Chem. Phys.* **2017**, *19*, 30166–30172.

[119]Kalhara Gunasooriya, G. T. K.; Saeys, M. CO Adsorption Site Preference on Platinum: Charge Is the Essence. *ACS Catal.* **2018**, *8*, 3770–3774.

[120]Figueiredo, M. C.; Hiltrop, D.; Sundararaman, R.; Schwarz, K. A.; Koper, M. T. M. Absence of diffuse double layer effect on the vibrational properties and oxidation of chemisorbed carbon monoxide on a Pt(111) electrode. *Electrochim. Acta* **2018**, *281*, 127–132.

[121]Dunwell, M.; Wang, J.; Yan, Y.; Xu, B. Surface enhanced spectroscopic investigations of adsorption of cations on electrochemical interfaces. *Phys. Chem. Chem. Phys.* **2017**, *19*, 971–975.

[122]Trasatti, S.; Lust, E. In *Modern Aspects of Electrochemistry*; White, R. E., J. O'M. Bockris, B. E. C., Eds.; KluwerAcademic/PlenumPublishers: New York, Vol. 33.
[123]Górniak, R.; Lamperski, S. On the influence of physical parameters on the properties of the electric double layer modelled by soft potentials. A Monte Carlo study. *Electrochim. Acta* **2018**, *286*, 279–286.
[124]Garlyyev, B.; Xue, S.; Watzele, S.; Scieszka, D.; Bandarenka, A. S. Influence of the Nature of the Alkali Metal Cations on the Electrical Double-Layer Capacitance of Model Pt(111) and Au(111) Electrodes. *J. Phys. Chem. Lett.* **2018**, *9*, 1927–1930.
[125]Zhu, J.; Xu, Y.; Wang, J.; Lin, J.; Sun, X.; Mao, S. The effect of various electrolyte cations on electrochemical performance of polypyrrole/RGO based supercapacitors. *Phys. Chem. Chem. Phys.* **2015**, *17*, 28666–28673.
[126]Wernersson, E.; Kjellander, R.; Lyklema, J. Charge Inversion and Ion-Ion Correlation Effects at the Mercury/Aqueous MgSO4 Interface: Toward the Solution of a Long-Standing Issue. *J. Phys. Chem. C* **2010**, *114*, 1849–1866.
[127]Schizodimou, A.; Kyriacou, G. Acceleration of the reduction of carbon dioxide in the presence of multivalent cations. *Electrochim. Acta* **2012**, *78*, 171–176.
[128]Ramírez, P.; Andreu, R.; Cuesta, A.; Calzado, C. J.; Calvente, J. J. Determination of the potential of zero charge of Au(111) modified with thiol monolayers. *Anal. Chem.* **2007**, *79*, 6473–6479.
[129]Morales-Guio, C. G.; Cave, E. R.; Nitopi, S. A.; Feaster, J. T.; Wang, L.; Kuhl, K. P.; Jackson, A.; Johnson, N. C.; Abram, D. N.; Hatsukade, T.; Hahn, C.; Jaramillo, T. F. Improved CO2 reduction activity towards C2+ alcohols on a tandem gold on copper electrocatalyst. *Nature Catalysis* **2018**, *1*, 764–771.
[130]Clark, E. L.; Resasco, J.; Landers, A.; Lin, J.; Chung, L.-T.; Walton, A.; Hahn, C.; Jaramillo, T. F.; Bell, A. T. Data Acquisition Protocols and Reporting Standards for Studies of the Electrochemical Reduction of Carbon Dioxide. *ACS Catal.* **2018**, *8*, 6560–6570.
[131]Wuttig, A.; Surendranath, Y. Impurity Ion Complexation Enhances Carbon Dioxide Reduction Catalysis. *ACS Catal.* **2015**, *5*, 4479–4484.